Advanced Computational Physics Lab. – Project 2

Heiko Menzler

October 18, 2022

1 Sum Product Belief Propagation in the 1D Ising Model

1.1 Cavity equations

To find the recursive cavity equations for $\omega_{i-1}^{(i)}$ in terms of $\omega_{i-2}^{(i-1)}$ we insert Equation (9) from the Exercise sheet into Equation (8). From this we get expressions for $P^{(i)}(\sigma_{i-1})$ that we can finally use in Equation (10) to obtain the recursive cavity equations

$$\omega_{i-1}^{i} = h + \frac{1}{2\beta}\log\left(\frac{\cosh(\beta) + \tanh\left(\beta\omega_{i-2}^{(i-1)}\right)\sinh(\beta)}{\cosh(\beta) - \tanh\left(\beta\omega_{i-2}^{(i-1)}\right)\sinh(\beta)}\right).$$

1.2 & 1.3 1D Chain propagation

Executing the sum product belief propagation algorithm on the 1D chain is very straight forward. As every site only ever has one other neighbor the cavity precisions propagate along the chain during the algorithm. For the initial cavity condition we choose $P^{(2)}(\sigma_1 = \pm 1) = 1/2$ ($P^{(2)}(\sigma_1 = +1) = 3/4$), which is equivalent to choosing $\omega_1^2 = 1$ ($\omega_1^2 = \log(3)$).

In Figure 1 the behavior of the algorithm is highlighted. We can see that the initial value does not have an impact on the final value that the algorithm converges against. This shows that we can find a fixpoint ω^* for given h and β that we will use in further analysis of the system.

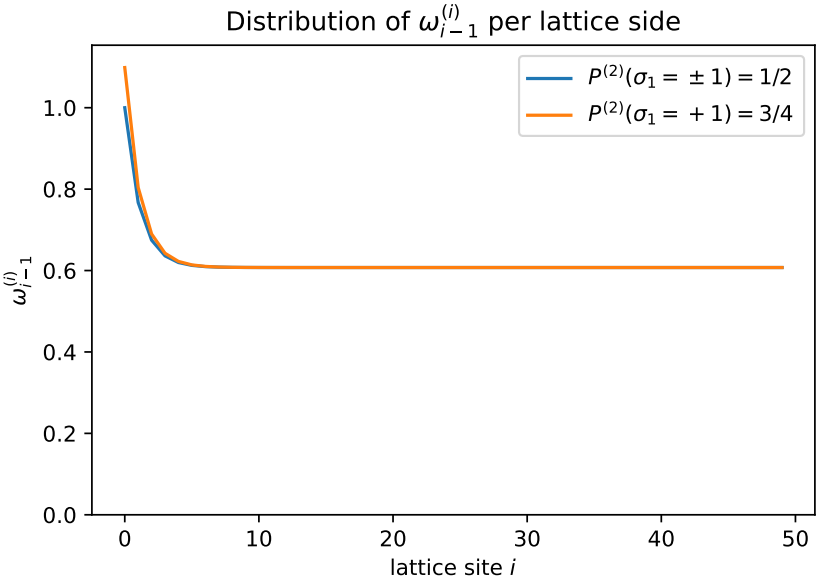

(a) Solution Ex. 1.2 & 1.3

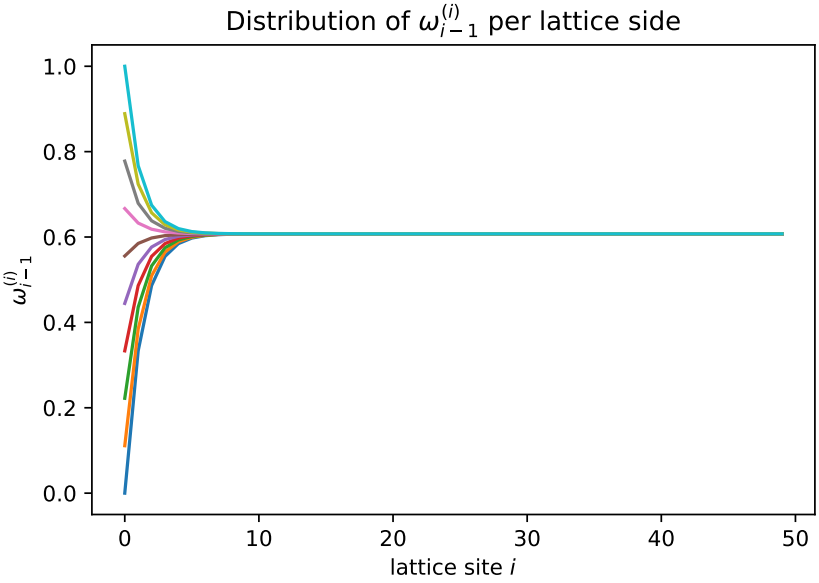

(b) Qualitative dependence on initial condition

Figure 1: These figures show the cavity precisions $\omega_{i-1}^{(i)}$ on the lattice for different initial cavity conditions. In Figure (a) one can see the required solutions to Ex. 1.2 & 1.3 while in Figure (b) one can see the cavity precision propagation through the lattice for ten different starting values. This highlights the qualitative behavior of the algorithm.

1.4 Magnetization in Thermodynamic Limit

In the thermodynamic limit we would expect that the algorithm will indeed converge to a fixpoint as we have seen in Figure 1. Due to the workings of the algorithm in the 1D case, to find this fixpoint in our problem we can simply take the cavity precision value of the last site in our chain.

This fixpoint can now be used to calculate the cavity probabilities and from these the actual probabilities. Such, we can calculate the order parameter of the system, which is the Magnetization M

$$\langle M \rangle = \frac{1}{N} \sum_{j=1}^{N} \langle \sigma_j \rangle \qquad \text{with} \qquad \langle \sigma_j \rangle = P(\sigma_i = +1) - P(\sigma_i = -1).$$

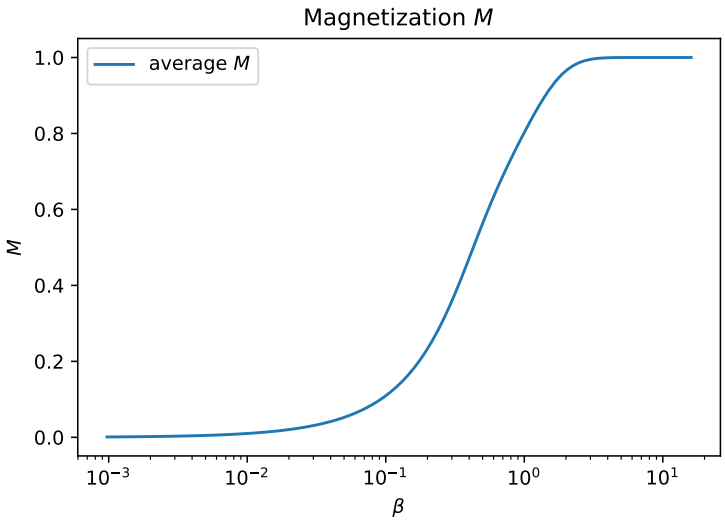

Figure 2: This figure shows the average Magnetization of the system plotted against the inverse temperature β. The critical point as given by the theory of phase transition is at $T = 0$.

In Figure 2 one can see that the average magnetization decreases for higher temperatures (lower β). We can verify that the analytical result [1]

$$m(\beta) = \frac{\sinh(\beta)}{\sqrt{\cosh^2(\beta) - 2e^{-2\beta}\sinh(2\beta)}},$$

coincides with the results obtained by our cavity method. Thus we have shown that the cavity method could be capable of yielding accurate solutions to one-dimensional problems. Unfortunately this is not a very strong

statement, yet, but we will try to build on this in further inquiries of the other exercises.

2 Random Matrix Theory

A lot of physical systems – e.g. systems with glassy dynamics – can often be modeled using graphs. This makes graph theory an integral part of physics itself and it has been studied extensively. In this exercise we will look at such systems that additionally contain disorder. Every regular graph can be expressed as an adjacency matrix which can be used to analyze the system.

2.1 Analysis by Direct Diagonalization

2.1.1 Sparse Random Matrix

In the first step of our analysis we use well known techniques to establish a baseline for our methodology. The method we use is called Direct Diagonalization and it obtains the spectrum of the system by using numeric Exact Diagonalization (ED).

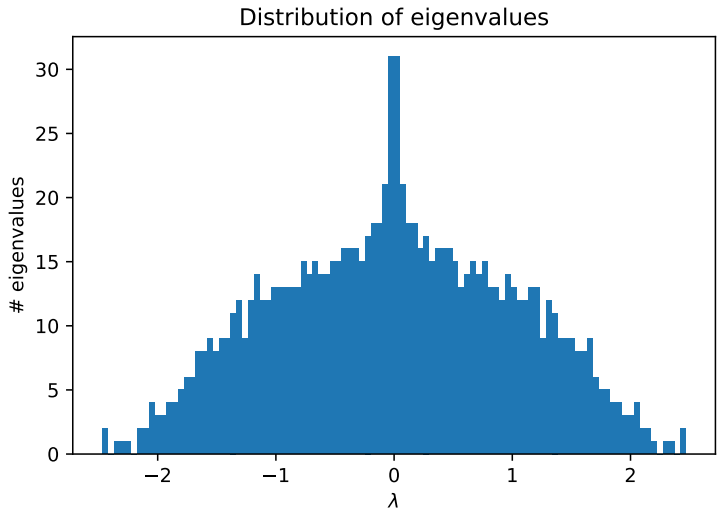

Figure 3: Spectrum of a RRG of size 2^{10} with connectivity 3 averaged over 10 different realizations.

In a first analysis step we generate 10 different Random Regular Graphs (RRG) and calculate their spectrum vie ED and average their spectrum. In Figure 3 you can see the spectrum of the RRG's adjacency matrices of size $N = 2^{10}$ with connectivity 3 averaged over 10 different realizations.

2.1.2 Fully Connected Graph

Next we want to analyze the spectrum of a fully connected network. For this we gain generate an adjacency matrix multiply it's components with gaussian noise scaled by $c = N - 1$.

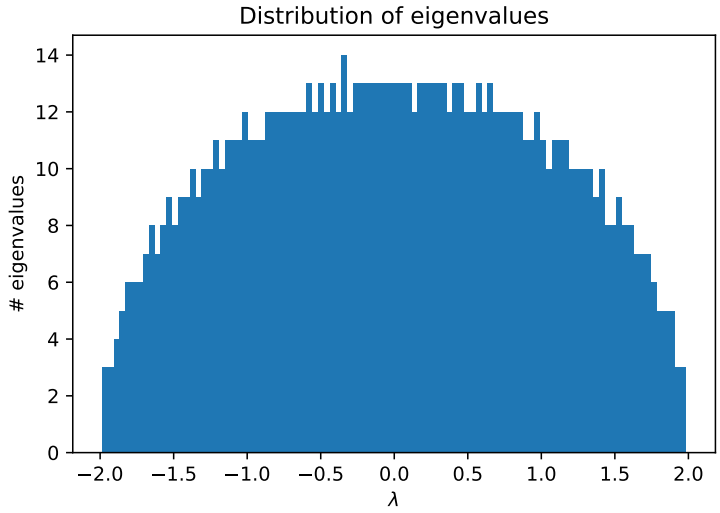

Figure 4: Spectrum of a fully connected network of size $N = 2^{10}$ ($c = N - 1$) averaged over 10 different realizations.

In Figure 4 we can see the spectrum of the fully connected network averaged over 10 realizations of the Random Graph.

2.1.3 Large Matrix limit

As the number of nodes in the fully connected graph increases we expect the self-averaging effects of the system to become stronger. This means that the density of our spectrum will more closely the exact solution in the $N \to \infty$ limit. That solution is given by the Wigner-Semicircle law, which states that the density of eigenvalues describes a semicircle described by

$$\rho(\lambda) = \frac{\sqrt{4 - \lambda^2}}{2\pi}. \tag{1}$$

2.1.4 Universality Classes

As graphs with a high connectivity c have very similar topology and their behavior is self-averaging, we can classify them by their spectral properties.

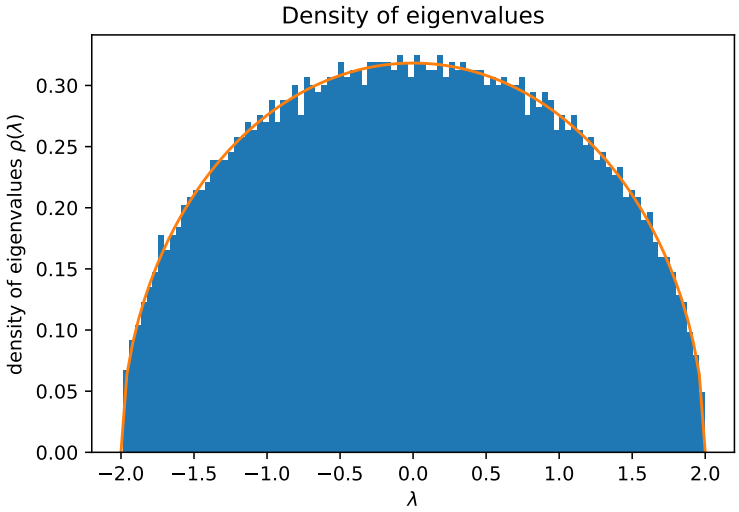

Figure 5: *Spectral density* of a fully connected network of size $N = 2^{12}$ of a single realization of a single realization. Furthermore we overlayed the semicircle defined given by the Wigner-Semicircle law from eq. (1).

In Figures 6a-6c we can see that already for quite small connectivities we get spectra that look very close to a semi-circle. We can see that our idea that high connectivities should belong to the same class of spectrum does clearly hold.

2.2 Analysis by Cavity Method

2.2.5 Update equation for the cavity precisions

To calculate the cavity precisions of the Random Matrix problem we again impose gaussian distributions for our cavity and marginal probabilities. This allows us to obtain recursive relations for the cavity and marginal precisions (inverse variances).

We can easily do so by inserting our assumptions into equations (18) and (19) on the exercise sheet. The resulting equation for the cavity precision $\omega_k^{(j)}$ at some site k, given some cavity at site j is

$$\omega_k^{(j)} = i(\lambda - i\epsilon) + \sum_{l \in \partial k \setminus j} M_{kl}^2 / \omega_l^{(k)}. \tag{2}$$

M_{kl} is the value of the given random adjacency matrix representing the edge between site k and l.

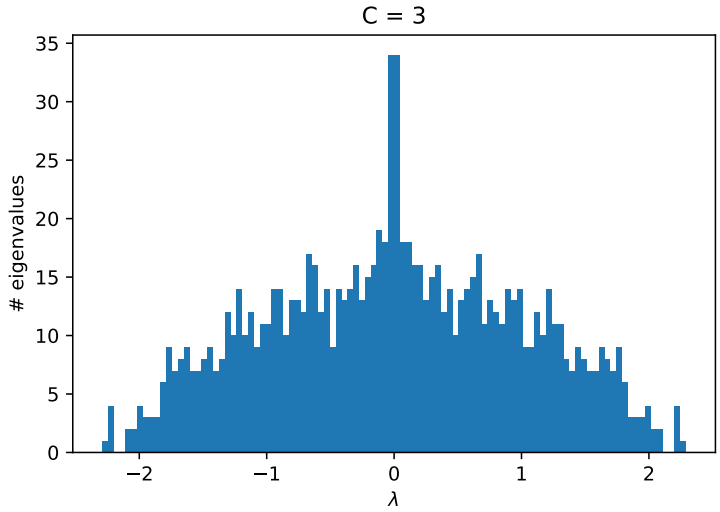

(a)

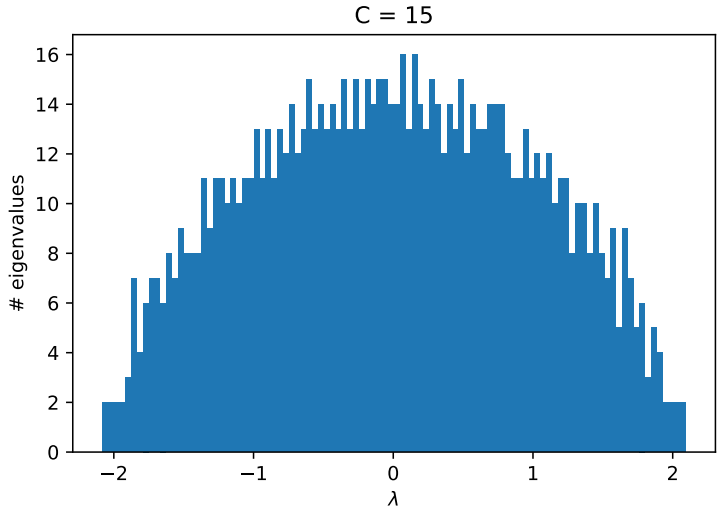

(b)

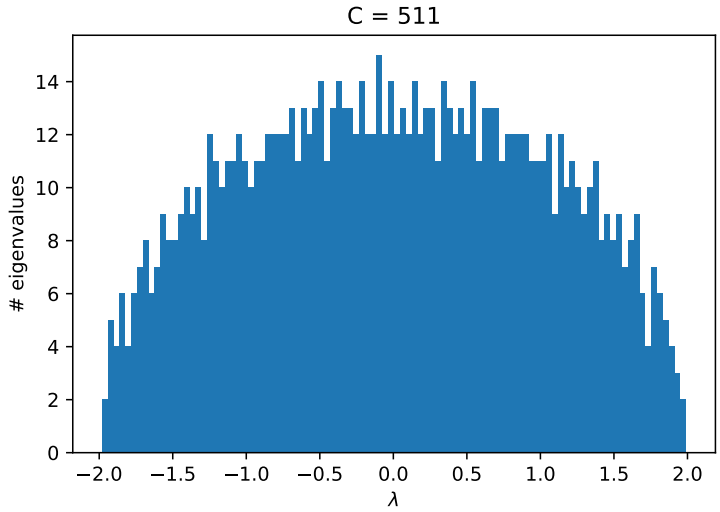

(c)

Figure 6: Spectrum of RRGs of size $N = 2^{10}$ with different connectivities c.

In similar fashion we can also obtain an equation for the marginal precisions ω_k at site k

$$\omega_k = i(\lambda - i\epsilon) + \sum_{l \in \partial k} M_{kl}^2 / \omega_l. \tag{3}$$

2.2.6 Cavity method for sparse matrices

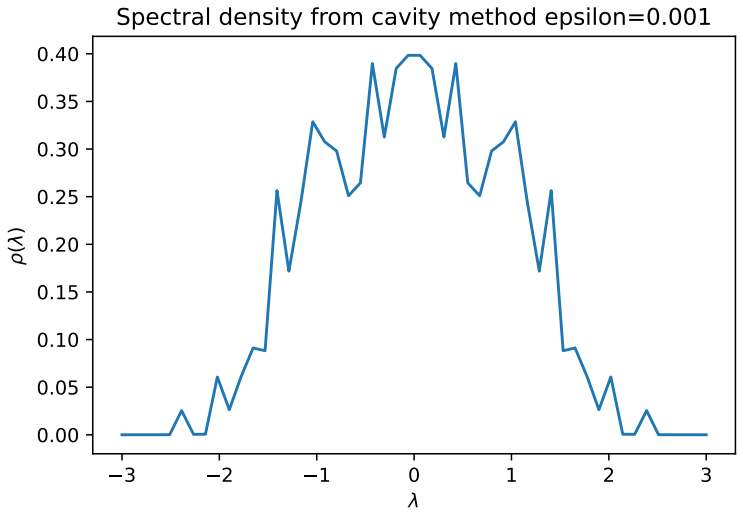

Figure 7: Spectral density calculated from the Cavity Method for $\varepsilon = 10^{-3}$ in a sparsely connected RRG of connectivity $c = 3$. The graph is made up from 2^{11} nodes.

Next to the method of direct Diagonalization we can also use the cavity method to obtain the spectrum of the graph's adjacency matrix. The spectrum shown in Figure 7 was obtained using this method using the cavity equations (2) and (3). We find that the spectrum is qualitatively consistent with the results obtained from Direct Diagonalization in Figure 3.

In Figure 8 we have displayed that same spectrum calculated using the cavity method but for different values of ε. We can see that the spectra from this version of the algorithm are slightly different to the one obtained for a larger ε. As to what the role of ε in the algorithm we feel that these results are inconclusive. Nonetheless we suspect that ε influences the convergence behavior of the algorithm and both Plots in Figure 8 show poorly converged spectra.

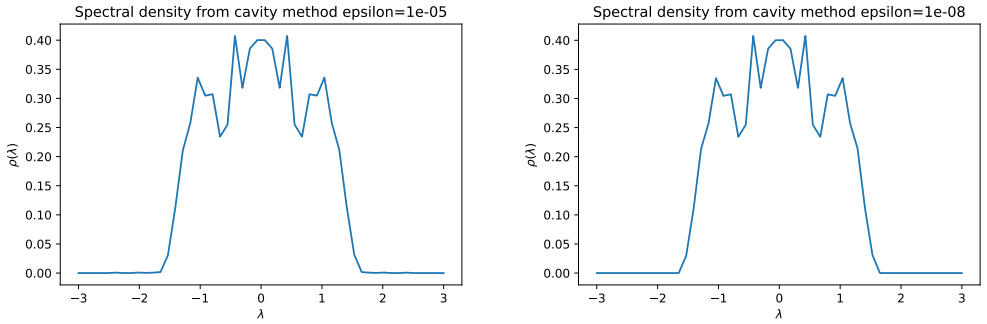

(a) (b)

Figure 8: Spectrum of the system for different parameters of $\varepsilon = 10^{-5}(10^{-8})$ in figure (a)/(b). Similar to Figure 7 the size of the graph is 2^{11} and the connectivity is $c = 3$.

2.2.7 Mean-Field limit

In the mean-field limit for the fully connected graph we assume $N \to \infty$. We can see from equation (2) that – in this limit and on a fully connected graph – the single term left out scales as $\mathcal{O}(1)$, while the entire sum scales as $\mathcal{O}(N)$. As N grows, we will find that it will be increasingly less significant whether we will be looking at the marginals or the cavity distributions.

2.2.8 Mean Resolvent

Another means to verify our results is by analyzing the system analytically in the mean field limit introduced in Section 2.2.7. We do so by analyzing the mean resolvent g and expressing it in terms of the marginal precisions ω_j

$$g_{\mathrm{MF}} = \frac{i}{N} \sum_{j=1}^{N} \omega_j^{-1}. \tag{4}$$

Into equation (4) we the obtained recursive relationship for the marginal precisions from equation (3). By using that $A_{ij} = 1$ in $M_{ij} = A_{ij} J_{ij}$ we can simplify the obtained equation to get

$$g_{\mathrm{MF}} = \frac{i}{N} \sum_{j=1}^{N} \left(i(\lambda - i\varepsilon) + \sum_{k \in \partial j} \frac{J_{kj}^2}{\omega_k} \right)^{-1}. \tag{5}$$

As we are using the fully connected case we can resolve the sum inside

the parenthesis in equation (5) to obtain

$$g_{\mathrm{MF}} = \frac{1}{N} \sum_{j=1}^{N} \frac{1}{i(\lambda - i\varepsilon) + \frac{1}{N} \sum\limits_{k}^{N} \frac{1}{\omega_k}}. \tag{6}$$

Such we have found the self-consistent equation (by identifying the sum of the denominator in equation (6) with g_{MF}). This equation is nothing more than then a quadratic equation in the mean field resolvent

$$g_{\mathrm{MF}} = \frac{i}{i(\lambda - i\varepsilon) - i g_{\mathrm{MF}}} \qquad \Longleftrightarrow \qquad g_{\mathrm{MF}} = \frac{\lambda_\varepsilon}{2} \pm \sqrt{\frac{\lambda_\varepsilon^2}{4} - 1}, \qquad \lambda_\varepsilon = \lambda - i\varepsilon.$$

If we plug this result into the given equation for the spectral density we recover the Wigner-Semicircle law

$$\rho(\lambda) = \lim_{\varepsilon \to 0} \mathrm{Im} \left(\frac{\lambda_\varepsilon}{2} \pm \sqrt{\frac{\lambda_\varepsilon^2}{4} - 1} \right) = \frac{1}{2\pi} \sqrt{4 - \lambda^2}.$$

Such we have shown that our simulation techniques are indeed consistent with analytical results.

3 Anderson Model

The Anderson Model was one of the first models that incorporated randomness when it was first proposed. It tries to model systems that have irregular or unforeseeable impurities in the Hamiltonian.

Generally the Anderson Model implements a tight-binding Hamiltonian with next-neighbor hopping. In addition to the hopping mechanism we add a small random potential at every lattice site. The microscopic Hamiltonian is

$$\mathcal{H} = -\sum_{\langle ij \rangle} c_i^\dagger c_j + \text{h.c.} + \sum_i E_i c_i^\dagger c_i, \qquad \text{where} \qquad \rho(E) = \frac{1}{W}\Theta\left(\frac{W}{2} - E\right).$$

When randomly introduced disorder becomes too large in this system, the system starts to localize and particles stop diffusing throughout the lattice. In this part of the Lab Course we want to study this process with the methods that we have acquired from the previous exercises.

3.1 Spectrum

From the spectral density of the system we can interpolate it's properties: In the tight-binding model we find $\rho(E = E_0) \ll 1$ ($E_0 \approx 0$ in the Anderson Model) while the edges of the density of states $E_0 \pm 2t$ are much more frequently occupied. Using our methods we can calculate the spectral density of the system, which in turn is very closely related to the density of states. Such we can use our methods to analyze the localization behavior of the model.

3.2 Spectrum from Direct Diagonalization and Cavity Method

To obtain a solid understanding of the Anderson Model's spectrum and to check them for consistency we use different techniques to calculate the spectral density. Firstly we use the most straight-forward technique which is – in this case – Exact Diagonalization. In Figure 9 you can see the eigenvalues of the system plotted in a histogram. This gives us exactly the spectral density we are interested in.

In similar fashion we have plotted the results of the cavity method in Figure 10 such that we find the spectral density $\rho(\lambda)$ on the y-axis. We can see that both results are consistent with each other.

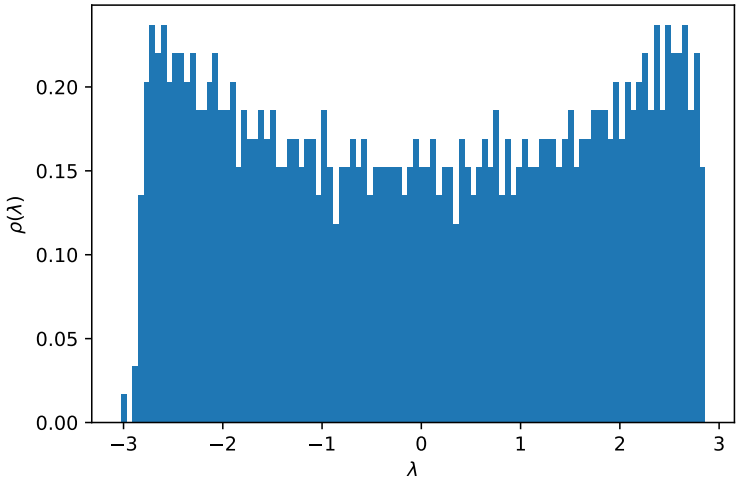

Figure 9: Spectral density of the Anderson Model for small disorder $W = 0.3$ on a large RRG of connectivity $c = 3$ and $N = 2^{10}$ nodes calculated by Direct Diagonalization of the Hamiltonian.

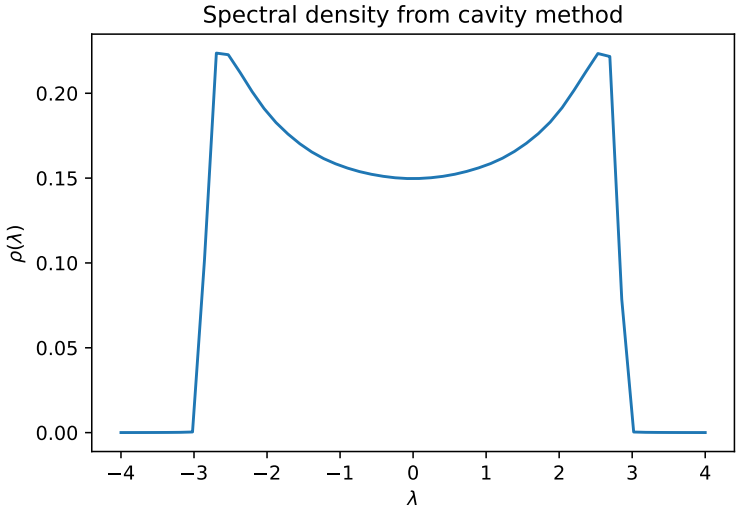

Figure 10: Spectral density of the Anderson Model for small disorder $W = 0.3$ on a large RRG of connectivity $c = 3$ and $N = 2^{10}$ nodes calculated by using the Cavity Method with $\varepsilon = 10^{-3}$ and the given cavity equations.

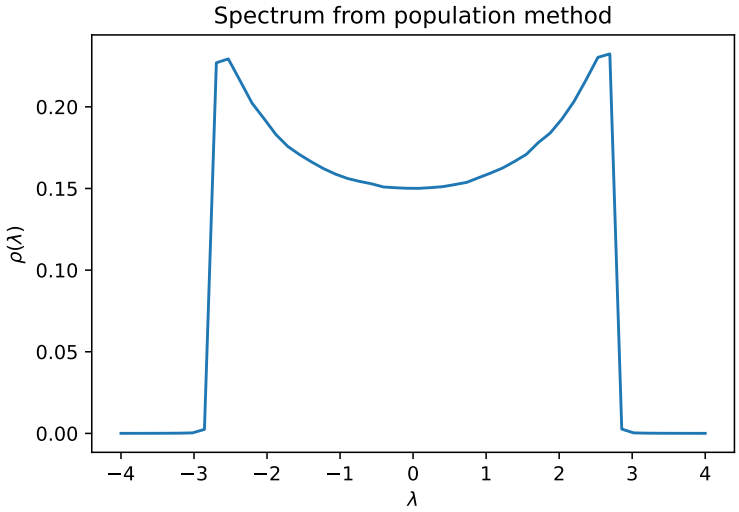

Figure 11: Spectral density of the Anderson Model for small disorder $W = 0.3$ on a large RRG of connectivity $c = 3$ and $N = 2^{10}$ nodes calculated by using the Population Method with $N_p = 10^3$ and the given cavity equations.

3.3 Spectrum from Population Method

We introduce another technique to analyze the system: The Population Method uses a population of cavity precisions to calculate the marginal precisions of the system. From Figure 11 we can clearly see that this technique is also consistent with the other methods we have used to calculate the spectrum of the Anderson Hamiltonian.

To ensure that the population of cavity precisions has reached equilibrium we use a stopping criterion. Such we stop, when a whole sweep (N_p updates) has not changed the absolute mean value of the cavity precisions by more than 10^{-4}. We are aware that this criterion is not universal, but throughout experimenting with the algorithm we have seen that this is criterion works sufficiently well.

3.4 Extended-Localized Transition – Cavity Variances

To look at the transition from extended to Localized States we can analyze the typical value of the cavity variances $g = {}^{i}\!/\!_{\omega}$, defined as $g^{\text{typ}} = e^{\langle \ln(\text{Im}\, g)\rangle}$. In Figure 12 we can see a steep drop-off (notice it's a log-plot) approaching the critical value of $W_c \approx 18.2$. As we are dealing with finite systems we want to look at the scaling behavior of different system sizes, which we can easily implement using the different population sizes. We can see that larger

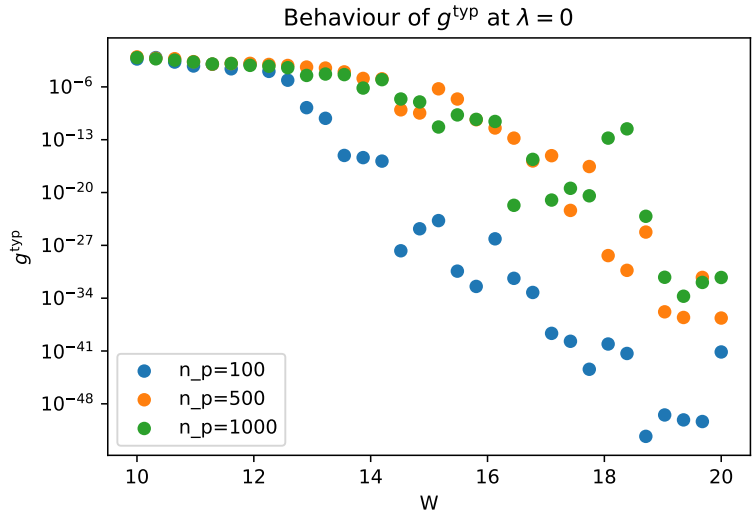

Figure 12: Scaling behavior of different population sizes of the typical cavity variance g^{typ} at different disoreder strengths using the population method for different population values N_p at $\varepsilon = 10^{-300}$ at fixed $\lambda = 0$.

systems make a much later transition (note that $N_p = 10^3$ starts decaying first and the other experiments generally have the larger values).

This transition can be understood as an isolator-conductor transition: At small disorder the system is in an extended state which allows for flow of "charge" between lattice sites. On the other hand – if the disorder becomes large – the system becomes localized and transitions between lattice sites are suppressed.

3.5 Extended-Localized Transition – Marginal Variances

To analyze the transition instead of looking at the Cavity Variances we can also look at the typical distribution of Marginal Variances for extended and localized states. In Figure 13 we can see that the typical distribution for localized state is strongly concentrated around 0 while the extended state can have a different mean and is generally more spread out.

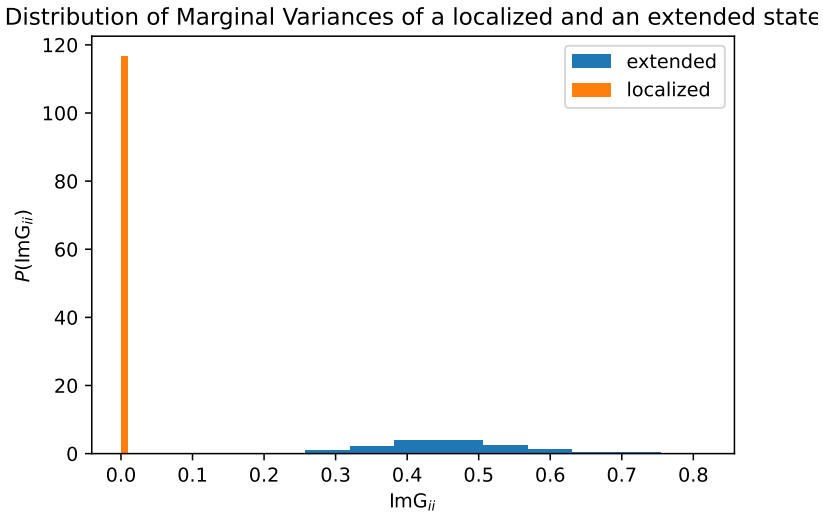

Figure 13: Marginal Variances distributions for a extended and for a localized state. The localized state was chosen at $W = 20$ and the extended state was chosen at $W = 2$. The Marginal Variances have been calculated from the Marginal Precisions of a Population Method simulation at $N_p = 10^4$ and $\varepsilon = 10^{-6}$

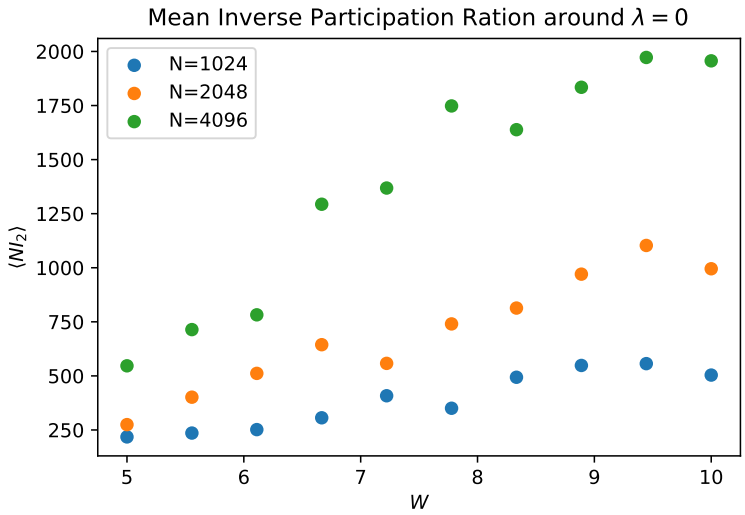

Figure 14: Average of the product $N \cdot I_2$ (I_2 being the IPR) over minimum 10 eigenvectors in a small environment around $\lambda = 0$ plotted against disorder strength W. The eigenvalues and eigenvectors for the different Graph sizes N were calculated using Direct Diagonalization.

3.6 Inverse Participation Ratio (IPR)

Lastly we want to look at the Inverse Participation Ratio (IPR)

$$I_2(v) = \frac{\frac{1}{N}\sum_{i=1}^{N} v_i^4}{\frac{1}{N}\sum_{i=1}^{N} v_i^2},$$

which is a well studied measure of how localized a given vector is (or conversely how spread out). Thus we might gain some further inside into the systems localization behavior by looking at this quantity. For the analysis we choose a few eigenvectors with eigenvalues around $\lambda = 0$ because they are most important for the conduction behavior.

In Figure 14 we can see the different scaling behaviors of the IPR values for different system sizes. We can see, that even though we have not chosen an interval of Ws with a transition we can still see that the IPR is scaling linearly (as we expect). Unfortunately this means that when we are looking at the transition, that we want to identify by using it's finite size scaling properties we need to distinguish between the natural scaling of the IPR and the finite size scaling of the transition. This means that the IPR measure is not very well suited to detect transitions in finite size systems.

References

[1] Ernst Ising. “Beitrag zur Theorie des Ferromagnetismus”. In: *Zeitschrift für Physik* 31.1 (Feb. 1925), pp. 253–258. DOI: 10.1007/bf02980577. URL: https://doi.org/10.1007/bf02980577.